Hindawi
Geofluids
Volume 2020, Article ID 8831544, 14 pages
https://doi.org/10.1155/2020/8831544

Research Article

Impinging Performance of High-Pressure Water Jets Emitting from Different Nozzle Orifice Shapes

Fei Huang,[1,2,3] **Jianyu Mi**,[3] **Dan Li**,[3] **and Rongrong Wang**[3]

[1]*Work Safety Key Lab on Prevention and Control of Gas and Roof Disasters for Southern Coal Mines, Hunan University of Science and Technology, Xiangtan, 411201 Hunan Province, China*
[2]*Hunan Provincial Key Laboratory of Safe Mining Techniques of Coal Mines, Hunan University of Science and Technology, Xiangtan, 411201 Hunan Province, China*
[3]*School of Resource Environment and Safety Engineering, Hunan University of Science and Technology, Xiangtan, 411201 Hunan Province, China*

Correspondence should be addressed to Fei Huang; fhuang@hnust.edu.cn

Received 15 June 2020; Revised 8 July 2020; Accepted 17 July 2020; Published 14 August 2020

Academic Editor: Yixian Wang

The impinging pressure of a water jet is a key factor in engineering applications, and the jet shape has a great influence on this pressure. In this paper, five different nozzle shapes were designed, and impacting tests were conducted based on a self-designed experimental platform using a PVDF piezoelectric film sensor and a high-speed camera to record the impacting data. Additionally, the computational fluid dynamics (CFD) method was also applied to study the velocity distribution. The results show that the pressure profiles of different water jet shapes impacting onto a solid surface present a consistent pattern, namely, an initial transient and enormous peak pressure and then a longer and smaller stagnation pressure. Although the stagnation pressure in this paper is not sufficiently obvious, the peak pressures of the five water jet shapes are much different from one another. Under the same inlet pressure, the peak pressure of the circular water jet is the largest, and those of the square, triangular, cross-shaped, and elliptical water jets decrease in turn. The flowing regimes captured by the high-speed camera together with the CFD simulation results indicate that the discrepancy in the peak pressure may be a combined action of the liquid velocities and jet head shapes.

1. Introduction

One of the most important developments in water jet technology is seeking out novel jets. As is known, the jet nozzle is one of the most important components of a water jet system. It is directly related to the shape and divergence properties of the water jet. Therefore, changes in the nozzle shape will bring about new types of water jets [1]. Recently, some special nozzles with noncircular outlets have been used in certain special applications, including agricultural irrigation, jet cleaning, and jet cutting. One of the most important features of noncircular jets is the axis switching phenomenon, in which the jet flow encounters a deformation around the streamwise axis after exiting around the nozzle. These noncircular outlet nozzles are collectively referred to as unconventional nozzles. As mentioned previously, the impacting pressure of a water jet is the key factor in engineering applications. Only if we gain their impacting performance can we use these unconventional jets in the engineering applications effectively. However, the impacting pressures and influence factors of these unconventional jets still are unknown at present.

Much attention has been given to researching unconventional nozzles. Singh et al. [2] experimentally investigated the entrainment characteristics of both circular and noncircular jets. They found that the jet with the cross-section of an isosceles triangle causes maximum entrainment. Yu et al. [3] conducted a numerical simulation on the jet entrainments of the circular, elliptical, square, cross-shaped, and triangular nozzles. It was determined that the maximum mean velocity time is a power function of the axial distance. Yang et al. [4]

proposed a combination of a square outlet, triangular outlet, and circular outlet to produce a better cavitation jet. Rouly et al. [5] designed an elliptical nozzle structure with variable axial parameters in order to obtain a high-pressure and low-divergence water jet, and three different nozzles with circular, rectangular, and elliptical outlets were designed to transmit the cutting fluid. The results showed that the circular nozzle has the best transmission performance, but it requires a higher inlet pressure [6]. Singh et al. [7] conducted experimental and numerical investigations to study the effects of the nozzle shape on unconfined jet impingement heat transfer from a heated circular cylinder. They selected circular, square, and rectangular nozzles of equal hydraulic diameters for a comparative study. Sodjavi et al. [8] investigated the characteristics of cross-shaped impinging jets and the resulting wall shear rates and mass transfer using electrodiffusion techniques and the particle image velocimetry (PIV) method. High-resolution PIV was also used to study the flow characteristics in the near field of rectangular, square, elliptic, and triangular water jets [9, 10]. Vouros et al. [11] conducted three-dimensional velocity measurements in the near field of a rectangular jet emanating from a sharp edge orifice. They found that the general evolution of the cross-sectional shape of the rectangular jet appears as a result of the corner vortices at the beginning of the jet. Vinze et al. [12] considered the influence of the nozzle shape (circular, square, and triangular) on the local heat transfer distribution and found that the mechanism of axis switching for noncircular jets is governed by the vorticity strength. Sharma and Fang [13] found larger widths and larger surface areas of diesel sprays from rectangular, square, and triangular orifices than those from circular orifices. Quinn [14] compared the mixing characteristics in the near field and transition region of a free jet from an elliptic orifice and circular orifice and found that the mixing in an elliptic jet emitting from a sharp-edged orifice plate is higher than in round jets.

The literature review indicates that the previous research on unconventional nozzles is mainly focused on the distribution of jet velocity, the flow field morphology, and the heat-mass transfer, with few papers having directly referred to the impacting performance of noncircular water jets as well as their influence factors. As we know, the impact-induced pressure and the impact dynamics can highly differ from those of a quasistatic case. What is more, the impact-induced pressure is not directly equal to the pump pressure (we use inlet pressure in the paper). Currently, it is generally accepted that the impact-induced pressure consists of two parts, namely, the water hammer pressure and the stagnation pressure. The former pressure usually several times larger than the inlet pressure plays an important role on the material destruction. The order of magnitude of this pressure depends on jet velocity, jet density, and jet shape. So, the main aim of this paper is to reveal the relationship between the water hammer pressure and the jet shape. As is known, the impact pressure, especially the central pressure of the impacting water jet, is of great importance in most of water jet applications [15–18]. Therefore, this paper intends to experimentally study the central impacting pressures of water jets issuing from different nozzle orifice shapes.

2. Basic Theory for Determining the Impact Pressure

When a high-pressure water jet impacts a solid surface, the velocity vectors of the high-speed fluid change, which may lead to a momentum loss of the water jet. As is known, this lost momentum will transfer to the impact force F acting on the solid surface. According to the momentum theorem, the impact force can be calculated as follows:

$$F = \rho Q v(1 - \cos\theta), \tag{1}$$

where ρ is the density of the fluid, Q is the rate of flow, v is the jet velocity, and θ is the angle between the wall surface and the reflecting direction of the fluid after impacting the object. The impact force F calculated by formula (1) is the total impact force of the jet acting on the solid surface. However, this impact force usually cannot directly reflect the ability of the jet breaking material. Generally, the impact force of a water jet onto a unit area of the material, i.e., the impact pressure, is actually a measurement of this ability.

This paper intends to use experimental methods to test the impact pressure P of water jets for different nozzle shapes. First, the total impact force F can be obtained by the pressure sensor. Then, the impact pressure P can be determined using the formula $P = F/A$, where A is the total contacting area of the water jet impacting on the solid surface. The total impact force F can be easily obtained through any number of test methods. However, the contacting area A varies greatly. This is due to the extreme complexity during the high-speed jet impacting onto the solid surface. One of the main complex problems is the variations in the cross-section of water jets. It is well known that a high-speed jet will mix with the surrounding air. This entrainment of the fluid with air will lead to a decrease in the boundary velocity of the water jet. Then, a jet structure with a large center velocity and a small boundary velocity forms, as shown in Figure 1. This velocity distribution will result in different impact pressures on the jet's cross-section. Therefore, the formula $P = F/A$ cannot be directly used to calculate the impact pressure.

For convenience, this paper assumes that the structure of the water jet is axisymmetric. For a certain jet cross-section, the center pressure is P_m and the impact pressure P_y at any point on this cross-section can be expressed as follows [19]:

$$\frac{P_y}{P_m} = \begin{cases} 1 - 3\left(\dfrac{y}{R_x}\right)^2 + 2\left(\dfrac{y}{R_x}\right)^3, & y \geq 0, \\ 1 - 3\left(\dfrac{y}{R_x}\right)^2 - 2\left(\dfrac{y}{R_x}\right)^3, & y < 0, \end{cases} \tag{2}$$

where y is the vertical distance from a point on the cross-section to the jet's center axis, and the value of y belongs to the range from $-R_x$ to R_x which is the radius of the jet on that section. Hence, the impact pressure at any point of the cross-section can be determined by the following expression:

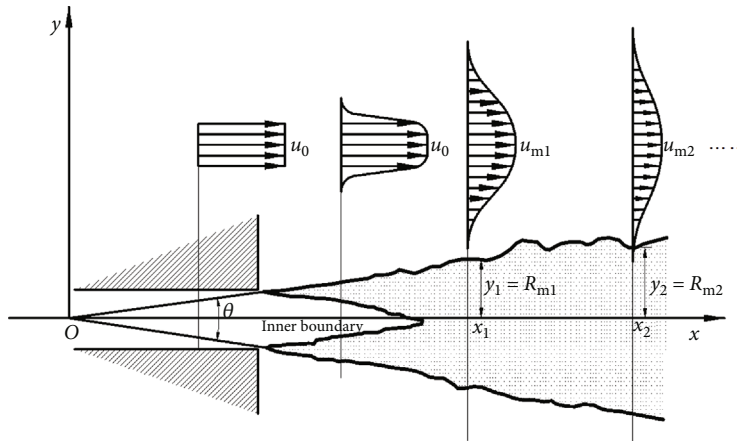

Figure 1: The structure diagram of a nonsubmerged water jet.

$$P_y = \begin{cases} \left(1 - 3Y^2 + 2Y^3\right)P_m, & 0 \le Y \le 1, \\ \left(1 - 3Y^2 - 2Y^3\right)P_m, & -1 \le Y < 0, \end{cases} \tag{3}$$

where $Y = y/R_x$. Obviously, the range of Y is between -1 and 1. Therefore, the total impact force of the section can be expressed as

$$\begin{aligned} F &= \int_0^Y \left(1 - 3Y^2 + 2Y^3\right)P_m dY + \int_{-Y}^0 \left(1 - 3Y^2 - 2Y^3\right)P_m dY \\ &= 2\left(|Y| - |Y|^3 + \frac{Y^4}{2}\right)P_m. \end{aligned} \tag{4}$$

In cases where the dimensionless variable Y is sufficiently small, the high-order terms in the above formula can be omitted, and it can be simplified into the following expression:

$$F \approx 2|Y|P_m. \tag{5}$$

Usually Y is considered a positive value due to the symmetry of jet structure; thus, the parameter Y in this paper is regarded as a positive one. Therefore, the center impact pressure can be approximately determined by the formula $P_m = F/2Y$. This calculation formula applies to nozzles with centrally symmetrical or axisymmetric jet structures.

3. Experimental Procedures

3.1. Experimental Platform. In this paper, five kinds of nozzles with different outlet shapes were designed: nozzles with circular, square, elliptical, cross-shaped, and triangular orifices. A unified internal structure including the convergence segment and line segment was applied to these nozzles as shown in Figure 2. The detailed parameters of the internal structure are illustrated in Table 1. It is assumed that the cross-sectional areas of all nozzles are equal to π mm^2. Hence, the equal hydraulic diameter is 2 millimeters, and the detailed structure sizes can be worked out, as shown in Figure 2.

To accurately capture the process of noncircular water jets impacting a solid surface, an experimental platform was set up, as depicted in Figure 3. This platform consists of two independent subsystems, which are the water jet-producing system and the data collection system. Firstly, water is pumped from the tank and pressurized to the experimental value in which 5 MPa, 10 MPa, 15 MPa, and 20 MPa are selected in this paper. Then, the pressurized water squirts from the nozzle to form a high-pressure water jet. As mentioned previously, this paper focuses on the transient behavior of the jet-solid impact. However, this water jet is continuously pressurized to a large value by the emulsion pump. Hence, how to generate the velocity-determined jet is a great challenge. In the present work, the pulse water jet generator designed by Dehkhoda and Hood [20] was applied with some modifications. The modified generator uses two solid circular plates to cut off the continuous jet. The front plate has two holes on the same circle and contra-rotates with the motor, and the back plate has a smaller hole and is fixed on the experimental platform. First, the positions of the holes on the front plate were adjusted to avoid the center of the nozzle. Thus, the unsteady water jet cannot pass through the hole. After the pressure of the water jet becomes steady, the front plate begins to rotate at a frequency f, driven by the motor. When the hole is on a line with the nozzle center, the continuous jet passes through the holes and a pulse water jet forms with a certain pressure. Note that the jet shapes, especially the jet head shapes, may change to irregular forms due to the rotation process. Hence, an optimal layout of the image acquisition system was selected in this experiment. In detail, the light source and camera should be in line with the jet beam firstly. Then, the light beam should be tangent to the rotation path of the hole on the cut-off plate. Under this condition, the captured jet shape under is kept consistent to that of the original jet shape which is dominated by the nozzle shape.

The angular frequency of the rotating plate is $\omega = 2\pi f$, and the central angle of the hole is θ. Hence, the duration of each pulse of the water jet can be obtained as

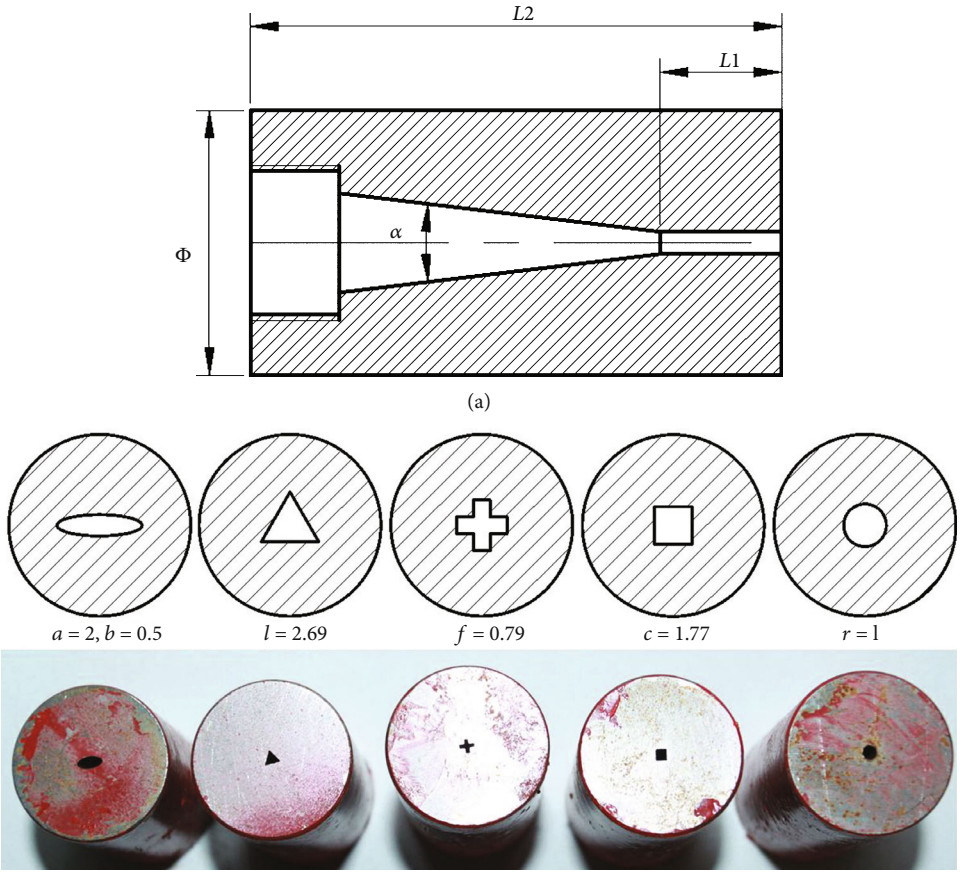

Figure 2: Internal structure and shapes of five different nozzles.

Table 1: Detailed parameters of nozzles.

Nozzle shape	Length of line segment L_1 (mm)	Length of nozzle L_2 (mm)	Convergence angle α (°)	Nozzle diameter Φ (mm)
Circular	11	48	14	24
Square	11	46	14	24
Elliptical	11	40	14	24
Cross-shaped	11	46	14	24
Triangular	11	44	14	24

$$\Delta t = \frac{\theta}{2\pi f}. \tag{6}$$

The data collection system is the key of this experiment. First, a piezoelectric polyvinylidene fluoride (PVDF) film is used to measure the total impact force F in this paper. Compared to some other pressure sensors, the PVDF film generates a high voltage by itself and has a thin and flexible structure, a high responsible frequency, a large range of linearity, and a low acoustic impedance. Additionally, it can be directly attached to the target body because of its extremely thin features. A PVF 4-.040-EK PVDF piezoelectric film was used in the present experiment [21]. The film sensor has a thin cylindrical size, with a 0.5 mm diameter and a 0.1 mm height, and it is covered by two silver plate electrodes soldered to a twisted wire pair. The application range of this film sensor can reach up to 10 GPa; thus, it completely meets the test demand in this work. As designed above, the equal hydraulic diameter is 2 millimeters. Hence, the dimensionless variable Y can be calculated by $Y = 0.5\,\text{mm}/2\,\text{mm} = 0.25$. Then, the pressure P_y is determined to be 0.84 times he pressure P_m according to formula (3). Here, P_y is the impact pressure of the water jet at the edge of the PVDF film, whereas P_m is that at the center of the PVDF film. In practice, the jet diameter expands with an increase in the axial distance, as shown in Figure 1. That is, the jet diameter is

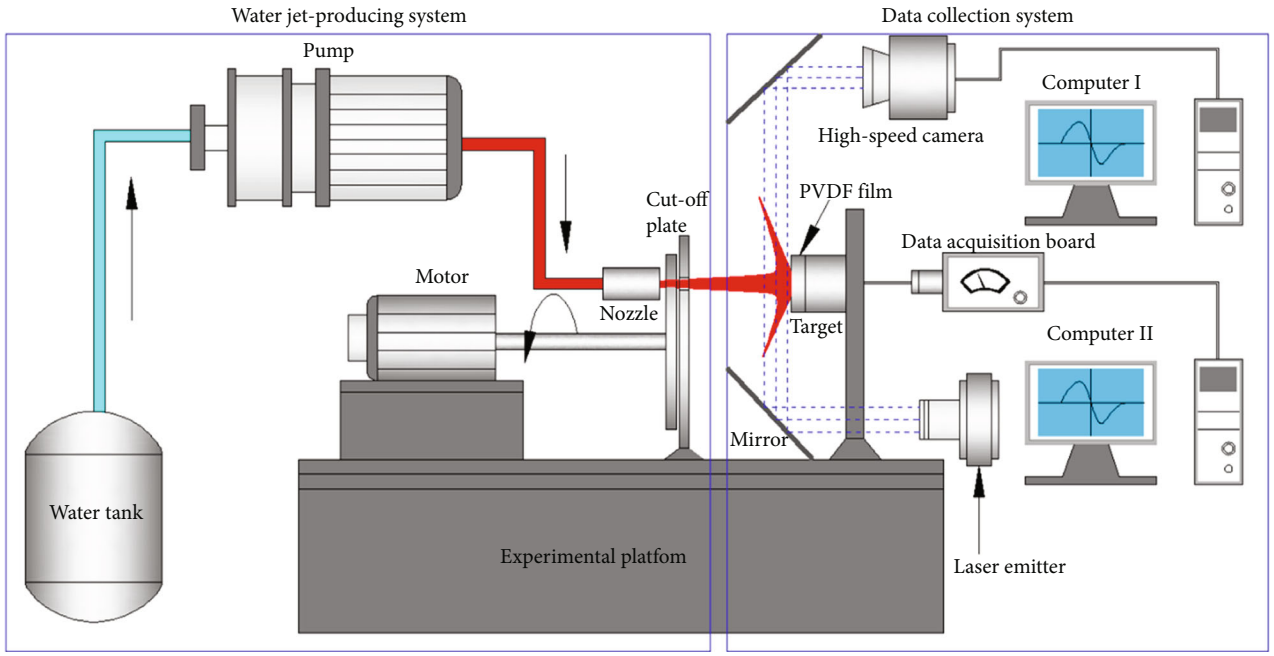

Figure 3: Schematics of the experimental setup used in the present study.

much larger than 2 millimeters and the dimensionless variable Y is smaller than 0.25. As a result, the measured pressure P_y is much larger than 0.84 times the center pressure P_m. Given that the impact pressure at the edge of the film is close to the center pressure, it is assumed that the PVDF film is subjected to a uniformly distributed pressure by the water jet. Hence, formula (5) can be used to calculate the center pressure P_m in this experiment.

In addition, an i-SPEED TR high-speed camera capturing as many as 10^4 frames per second was applied to capture the processes of the jets impacting on the solid surfaces. The camera was placed perpendicularly to the jet impacting direction. To protect the camera from the splash of the water jet, a cubic waterproof cover made of polymethyl methacrylate (PMMA) was placed around the camera. A binary algorithm was applied to process the images of the jets impacting the solid surfaces, which directly demonstrates the flow regime of the high-speed fluid after impacting onto the solid surface.

3.2. Numerical Simulation Validation. This paper intends to experimentally study the impacting performance of water jets with different cross-sections. As is known, the jet shape just at the nozzle exit is nearly the same as that of the nozzle orifice. However, these certain jet shapes can change with an increase in the axial distance due to air entrainment. Hence, the exact shape of the cross-section at a certain axial distance is unknown to us. Since we did not perform any velocity measurements, the velocity profile, which can directly illustrate the shape of the cross-section, cannot be determined by experimental methods. Therefore, a CFD method was applied to investigate the variations in the jet shapes from different orifices.

The numerical models were built up according to the experimental nozzles, as shown in Figure 4, of which the Y -axis is set as the jetting direction, the Z-axis is set as the vertical direction, and X-axis is set as the radial direction. The boundary condition consists of the pressure inlet, wall, and pressure outlet. Here, we set the nozzle inlet pressure to 15 MPa, and the nozzle outlet pressure is atmospheric. We can use these parameters as well as the velocity contour to numerically simulate the flow features outside the nozzle. The velocity distribution of the water jets at different axial distances can be acquired, as shown in Figure 5, in which X represents radial distance and Z represents vertical distance corresponding to the coordinate axis in Figure 4. D is the equal hydraulic diameter of water jets.

It can be seen from the velocity contour maps of the five different nozzles that the jet cross-section shapes are in accordance with corresponding nozzle orifices in the initial jet region, for example, the jet cross-section shapes at an axial distance of 3 mm. With an increase in the axial distance, all jet cross-sections are gradually transformed into circular shapes. As is known, circles, squares, and crosses are centrosymmetric, while triangles and ellipses are only axisymmetric. Finally, all of these jet cross-sections are centrosymmetric circles. Hence, the symmetries of the triangular and elliptical nozzles changed with an increase in the axial distance, which shows that the entrainment performances of these two jets are enhanced. According to the changes in the jet cross-section with an increase in the axial distance, a proper axial distance must be selected in order to keep the same shape as that of the nozzle orifice. Hence, a distance of 12 millimeters was chosen as the target distance in this experiment.

4. Results and Discussion

4.1. Flow Regimes of the Water Jets Impacting on the Solid Surface. The impinging performance of the water jet is jointly

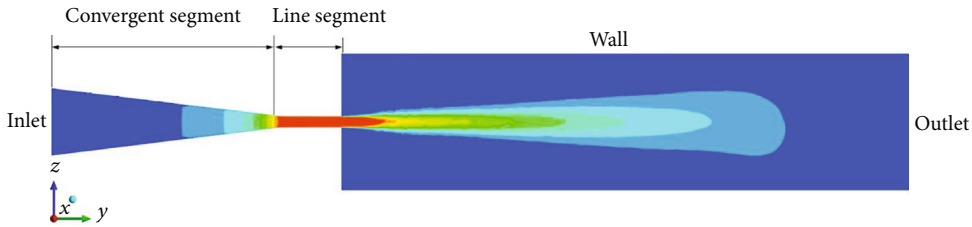

Figure 4: The configuration of the numerical model.

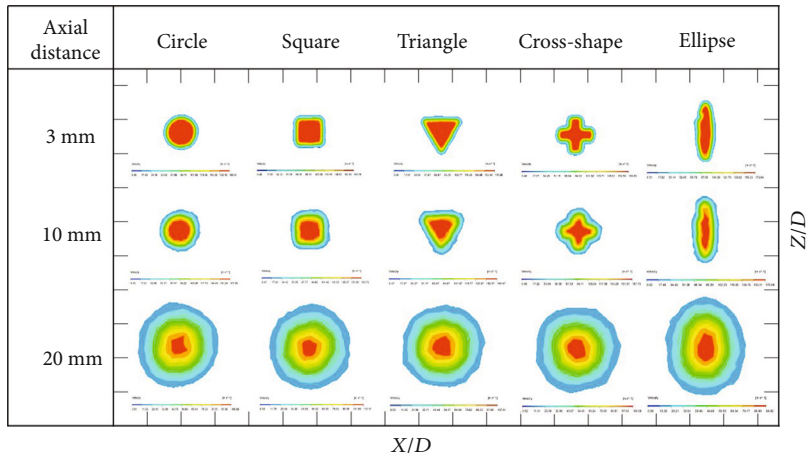

Figure 5: The velocity contour of the water jet at different distances.

impacted by many factors, of which the jet's structural features, including the flow field and velocity field, have drawn much attention during the past few decades. This is mainly because the jet structure has a direct influence on the impingement. However, the high-speed liquid to solid contacting process also has a great impact on the impinging pressure and especially on the transient pressure at the instant of the liquid contacting the solid surface. This point of view was initially proposed by Bowden and Field [22], and then a large amount of later studies [23] proved this assumption by both experimental and numerical methods. However, most of these studies either used a circle, like a liquid droplet, or simplified the jet into a cylinder. In practice, the jet head is irregular, as shown in Figures 5–9. Hence, the liquid-solid contacting process may present a great difference when an actual water jet is impacting, which may lead to a discrepancy in the impacting pressure.

Figures 6–10 are the binarized images of the water jets impacting the solid surfaces. Great discrepancies appear in the jet structures with variations in the nozzle shapes, especially the shape of the jet head. As mentioned above, all of the jet heads are irregular. This is in line with the experimental findings by Liu et al. [24]. Additionally, the jet heads from different nozzle orifices vary greatly from one another. First, the jet head from a circular orifice appears to be an umbrella-like shape, as outlined by the dotted line in Figure 6 when $t = 0.75$ ms. Note that the jet head is discontinuous when enlarging the image. In other words, it consists of many high-speed water drops. The umbrella-like shape is just an envelope curve of these water drops. Hence, the contacting process of the water jet impacting a solid surface is in fact that of many water drops impacting. This could be the root reason for the difference in the impacting pressure between an actual water jet and an ideal water jet with a continuous jet head.

Then, the jet head from a square orifice, as shown in Figure 7, appears as a mushroom-shaped umbrella with a much flatter head than the circular jet. This structure indirectly indicates that the circular jet is more convergent than the square jet. However, the remaining three jet heads are much different from the above situations. The jet head from the triangular orifice, as shown in Figure 8, looks like a fist, and its size is much smaller than those of the circular and square jets. The jet heads from the cross-shaped (Figure 9) and elliptical orifice (Figure 10) are both like enlarged arrows. However, the size of the cross-shaped jet is the smallest, while that of the elliptical jet is the largest. Of note is that all of these jet heads are discontinuous and consist of plenty of high-speed water drops.

In addition to the discrepancy of the jet head, the jet sections from different orifices are quite distinctive from one another. Irregular and smooth cylindrical beams appear when the jet emits from either a circular or square orifice, respectively. The jet section of the triangular jet is asymmetrical. From the two-dimensional images as shown in Figure 8, the lower side of the jet section is much smoother than that of the upper side. This could be caused by the shooting angle of the high-speed camera, which presents two extreme phenomena when the jet is emitting from an elliptical or cross-shaped orifice; namely, the width of the cross-shaped jet is

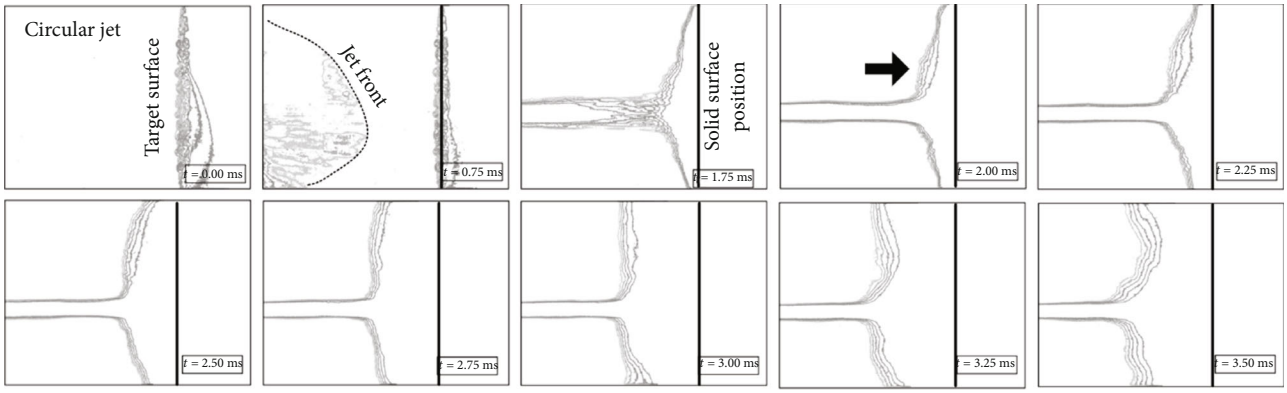

Figure 6: The evolutions of a circular jet impacting a solid surface.

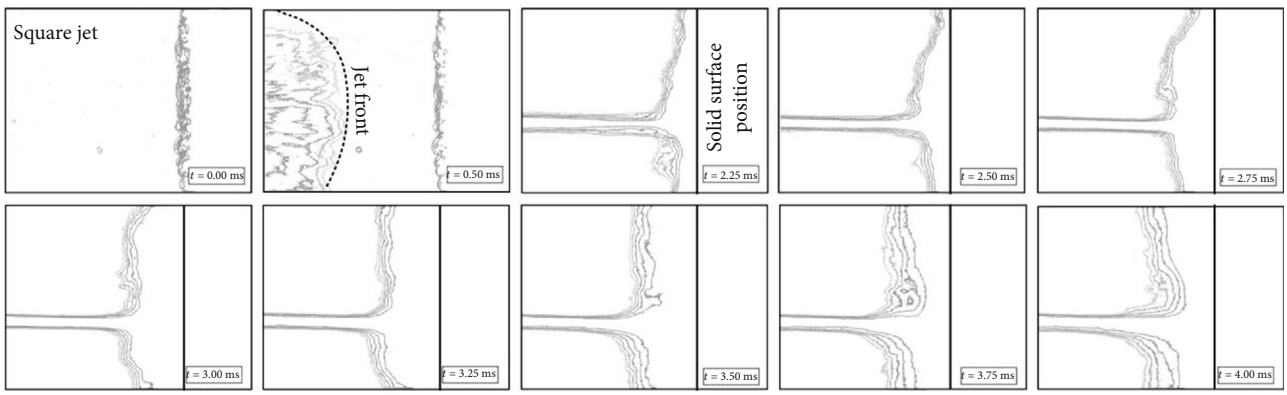

Figure 7: The evolutions of a square jet impacting a solid surface.

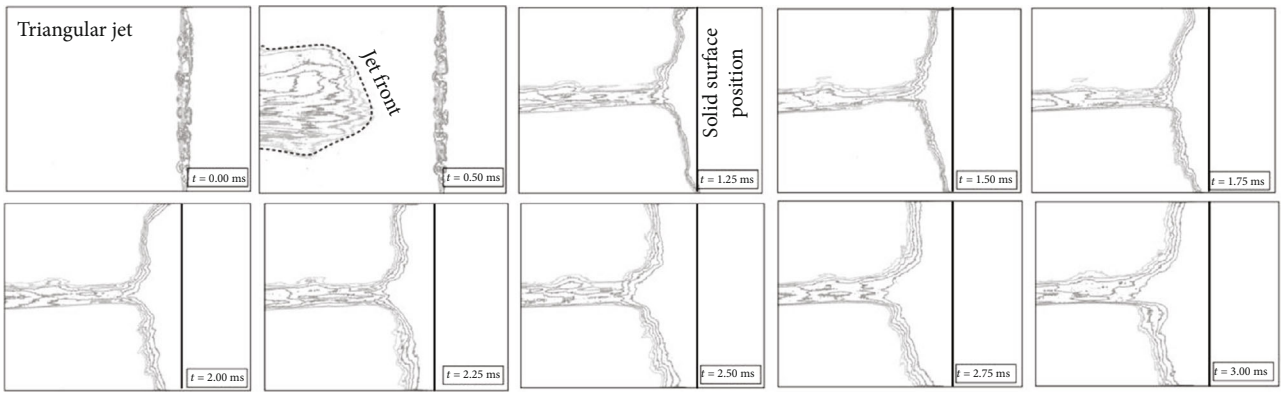

Figure 8: The evolutions of a triangular jet impacting a solid surface.

the smallest, while that of the elliptical jet is the largest. In this paper, we define the width of the target as 1. Hence, the normalized width of the jet from five different orifices can be obtained. In detail, the widths of the circular, square, triangular, cross-shaped, and elliptical jets are approximately 0.11, 0.08, 0.12, 0.06, and 0.35, respectively.

Accordingly, the obvious variations in the jet head and the main section of the water jet from different orifices may at last cause a great discrepancy in the jet-solid impacting process. These processes can be directly observed by the flow regime of high-speed fluids before and after contacting. From the high-speed camera images, it can be seen that a protruding part, as pointed by the arrow in Figure 6, appears immediately after the jet-solid contact. At this time, a typical flow regime with the center fluids protruding while the peripheral fluids are denting can be easily observed. As the jet-solid impacting continues, the protruding part moves outwards until it finally disappears. Then, a steady flow regime with a V-shape appears until the end of the impact. In the same way, all of the noncircular water jets impacting the solid

Figure 9: The evolutions of a cross-shaped jet impacting a solid surface.

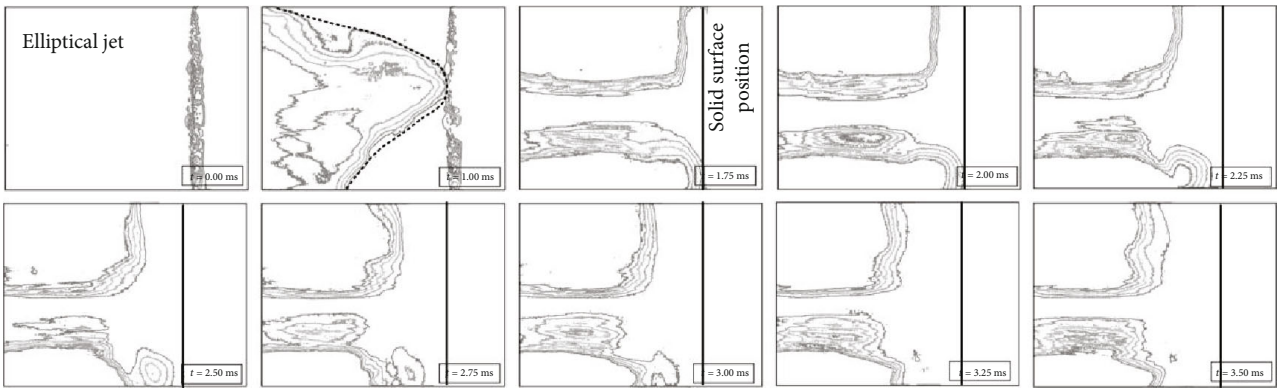

Figure 10: The evolutions of an elliptical jet impacting a solid surface.

present flow regimes similar to that of the circular water jet. However, certain differences exist among different water jets, such as the commencing point of the fluids protruding, the duration of the protruding part lasting, and the final V-like shape. Taken altogether, the foregoing flow regime of the circular water jet impacting the solid is most obvious, followed successively by those of the square jet, triangular jet, and cross-shaped jet. However, the flow regime of the elliptical jet impacting the solid shows only a little similarity with those of the other four water jets.

Analysis shows that these flow regimes are caused by the compression of fluids around the jet center. During the liquid-solid impact, only the liquid at the edge is free to flow initially, whereas the liquid at the center remains compressed until being reached by the release waves from the sides. This means that only if the liquid cannot freely flow outward may the liquid in this area protrude, as shown in Figure 6. Generally, a much higher liquid compression degree may cause a more obvious liquid protruding phenomenon, namely, a much larger protruding height and much longer duration. The liquid compression may at last induce a huge so-called water hammer pressure [25], and this liquid compression is jointly impacted by the shock wave, the liquid velocity, the jet shape, and so on [23, 26–28]. According to Huang et al. [23], the liquid-solid collision will induce a shock wave that will propagate against the impact direction in a compressive manner. It is implied that the compression wave spreading into the liquid must be attached to the edge's contact point by the classical Huygens principle. Due to the curved shape of the jet, the contact point moves outward onto the liquid-solid interface in advance of the shock. At this time, the liquid within the shock wave is extremely compressed, so a protruding part appears around the jet center. As the shock envelope expands outwards, the protruding part correspondingly moves outwards. Once the shock envelope detaches from the contact point, a lateral jet forms and the protruding part disappears.

As mentioned above, the jet shape, especially the jet head shape, plays a significant role in the liquid compression. Hence, the diversity of the head shapes of the water jets emitting from different orifices leads to the discrepancies in the flow regimes. According to the liquid-solid impacting images, the protruding part of the circular water jet is the most obvious, which implies that the umbrella-like head shape of the circular water jet is not conducive to the generation of the lateral jet and it may enhance the liquid compression degree. Similarly, the mushroom-shaped umbrella head shape of the square water jet may also cause a considerable liquid compression. By comparison, the head shapes of the triangular, cross-shaped, and elliptical water jets act differently on the compression degree. In detail, the fist-like head shape of the triangular jet induces asymmetric liquid

compression due to its structural features. This is the reason for the different flow regimes between the upper and lower sides of the triangular jet, as shown in Figure 8. In addition to the triangular jet, the head shape of the elliptical jet with a major axis and a minor axis also causes an asymmetric liquid compression. In the minor axis direction, the liquid is conducive to outward flow and suffers only minor compression. In contrast, the liquid in the major axis direction is greatly compressed. Although the head shape of the cross is axisymmetric, the actual diameter is much smaller than those of the other four shapes. Hence, the flow regimes of the cross-shaped jet reflect that its center compression degree is also sufficiently small. These flowing features may at last cause a great discrepancy in the impacting pressures.

4.2. Central Pressures of Different Jets Impacting a Solid Surface. As previously mentioned, this paper intends to investigate the impacting pressures at the center point of different jets impacting onto a solid surface. The total impacting force on the PVDF film subjected to a water jet can be recorded first, and then the central pressure can be approximately determined using formula (5). Then, the central pressure profiles of different water jets impacting are illustrated in Figure 11.

As seen from the pressure profiles, there is a consistent pattern for all water jet shapes. First, the central pressure climbs up to an enormous value in an extremely short time. The magnitude of this duration is on the order of approximately one millisecond. After the central pressure reaches the peak value, it decreases gradually to a relatively stable pressure and at last decreases to zero. This phenomenon nearly accords with the previous research results [29] in terms of the water jet impacting pressure, which proposed that the process of the water jet impacting can be divided into two typical stages, namely, the water hammer pressure stage and the stagnation pressure stage. Note that minor differences in the stagnation stage exist between the previous study and these experimental results. The former holds the opinion that the stagnation pressure is a steady value and it will last a relatively long duration, whereas the stagnation pressure in this experiment is not sufficiently obvious. We believe that this discrepancy is mainly caused by the acting duration. The former considered the impacting of the water jet as a continuous process, while this experiment used a pulsed water jet. The duration of each pulse is approximately 15 milliseconds according to formula (6). Hence, we believe Figure 11 is a typical pressure profile of a pulsed water jet impacting. This finding is roughly in line with the experimental results by Li et al. [30].

Another noticeable feature of the pressure profile is that the peak pressures of the five water jet shapes impacting solids are much different from one another, whereas the stagnation pressures are close to one another. Taking Figure 11(a) as an example, the peak pressure of the circular water jet impacting reaches as high as approximately 47 MPa when the nozzle inlet pressure is 5 MPa. Under the same nozzle inlet pressure, the peak pressures of the square, triangular, cross-shaped, and elliptical water jets impacting decrease in turn. By comparison, the minimum peak pressure of the elliptical water jet impacting is approximately 38 MPa, only reaching 80 percent of that of the circular water jet. This phenomenon does not change significantly with an increase in the nozzle inlet pressure.

To investigate the influence of the inlet pressure on the central peak pressures of different water jets, a controlled experiment was conducted selecting the inlet pressures of 5 MPa, 10 MPa, and 20 MPa. As is known, the peak value and duration are the two main parameters of the peak pressure. The peak values of all five water jet shapes increase nonlinearly with an increase in the inlet pressure, as shown in Figure 12(a). Note that the slopes of curves in Figure 12(a) decrease gradually with an increase in the inlet pressure, which reflect that the influence of the inlet pressure on the peak pressure decreases with an increase in the inlet pressure. The relationship of the peak pressure duration with the inlet pressure is shown in Figure 12(b). As illustrated in Figure 11, no obvious stagnation pressures appear for these pulsed water jets. Therefore, it is difficult for us to gain the duration from the starting time to the stagnation time. In this paper, we define the time interval from the starting point to the peak value point as the duration of the peak pressure. It can be seen from Figure 12(b) that the durations of all kinds of water jets are nearly kept constant with an increase in the inlet pressure. Another noticeable feature is that the durations of the cross-shaped and triangular water jets are much longer than those of the other three water jets.

4.3. Discussion of the Results. As mentioned previously, two main factors may account for the discrepancy of the peak pressure. Since the impacting pressure is the result of fluid kinetic energy, the liquid velocity plays an important role on the peak pressure. As pointed out by Lesser and Field [31], the peak pressure at the central area is given as

$$P = \rho C v, \tag{7}$$

where v is the liquid velocity and ρ is the density of the water. Ref. [32] gave the shock wave velocity C by the following relationship:

$$C = v_s + \varphi v, \tag{8}$$

where v_s and φ are the acoustic speed and the numerical parameter, respectively. For water with a velocity up to 1000 m/s, φ is set to 2. Hence, formula (7) can be written as $P = \rho(v_s + 2v)v$. It is assumed that the acoustic speed v_s is a constant in this experiment, and the peak pressure P is only a quadratic function of the liquid velocity v. In this experiment, we did not conduct the velocity measurements but set the same inlet pressure P_i for all kinds of water jets. To obtain the velocity distribution, the CFD method was used. The velocity distributions of different water jet shapes are shown in Figure 13. The impacting force measurement was conducted at a normalized distance of 7.5 Y/D as shown in Figure 13(a), where Y is the axial distance in millimeters and D is the equal hydraulic diameter of 2 millimeters. According to Figure 13(b), the central velocities of the five water jet shapes decrease with the normalized axial distance. The contour maps show that the cross-sections of all water jet

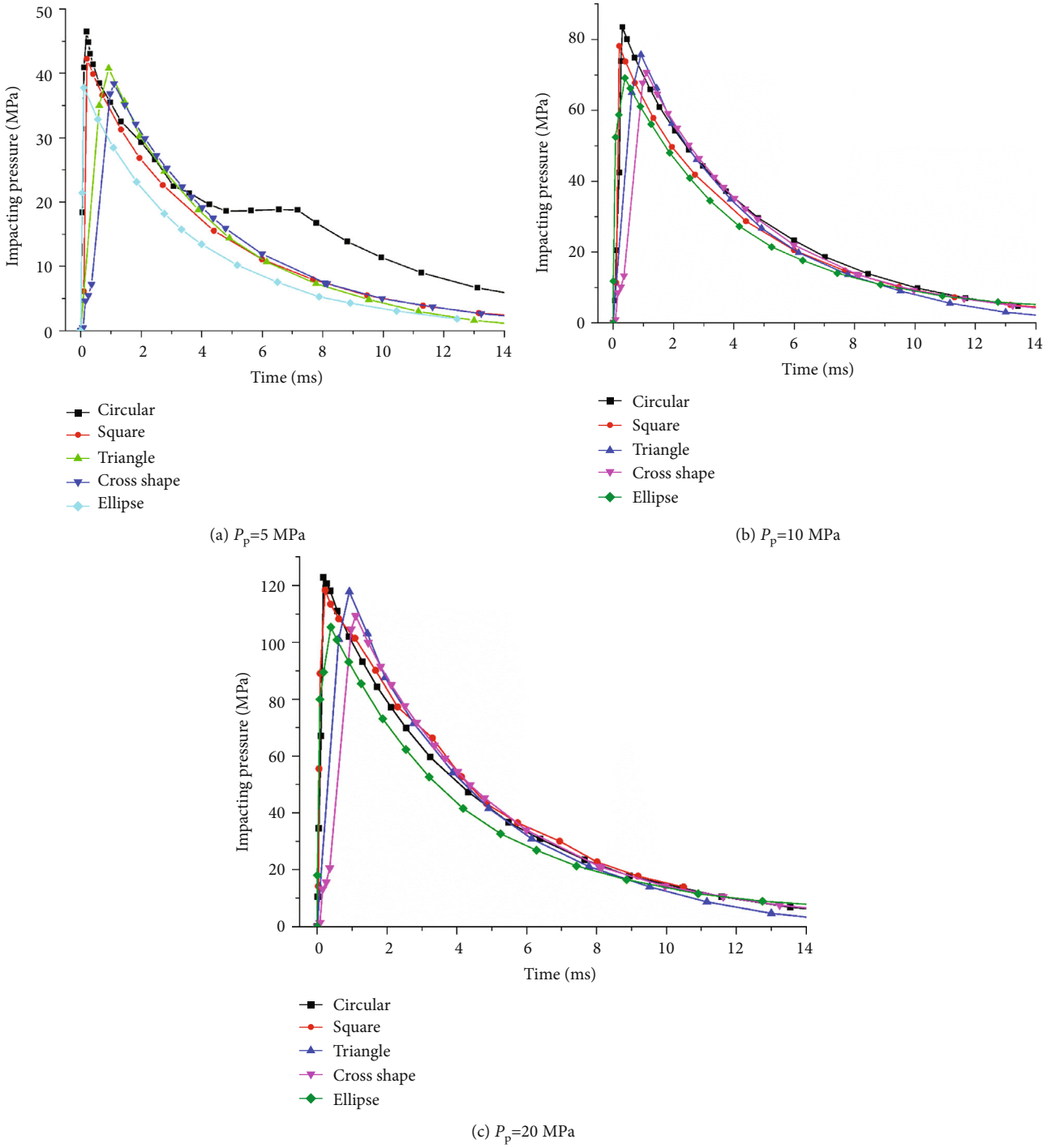

Figure 11: Pressure profiles of different water jets versus time.

shapes at this distance are in the extension segment where the radial velocity distribution is approximately normal, as shown in Figure 13(c). The diameter of the PVDF film is 0.5 millimeter corresponding to 0.25 Z/D, where Z is the radial distance in millimeters. Within this area, it is difficult for us to observe the detailed velocity distribution due to the overlap of curves, as shown in Figure 13(c). Therefore, an enlarged figure was collected in Figure 13(c). It can be seen that the central velocity of the circular water jet at this cross-section is the highest, whereas that of elliptical water jet is the lowest, and those of the square, triangular, and cross-shaped jets are in the middle. This velocity distribution is essentially consistent with that of the central pressure as shown in Figure 11. Hence, we can infer that the velocity distributions of the five water jet shapes are the main cause for the discrepancy of the peak pressure, giving the same nozzle inlet pressure.

In addition to the velocity distributions, the jet shape, especially the head shape, may be another reason for the discrepancy in the center pressure. According to the flow

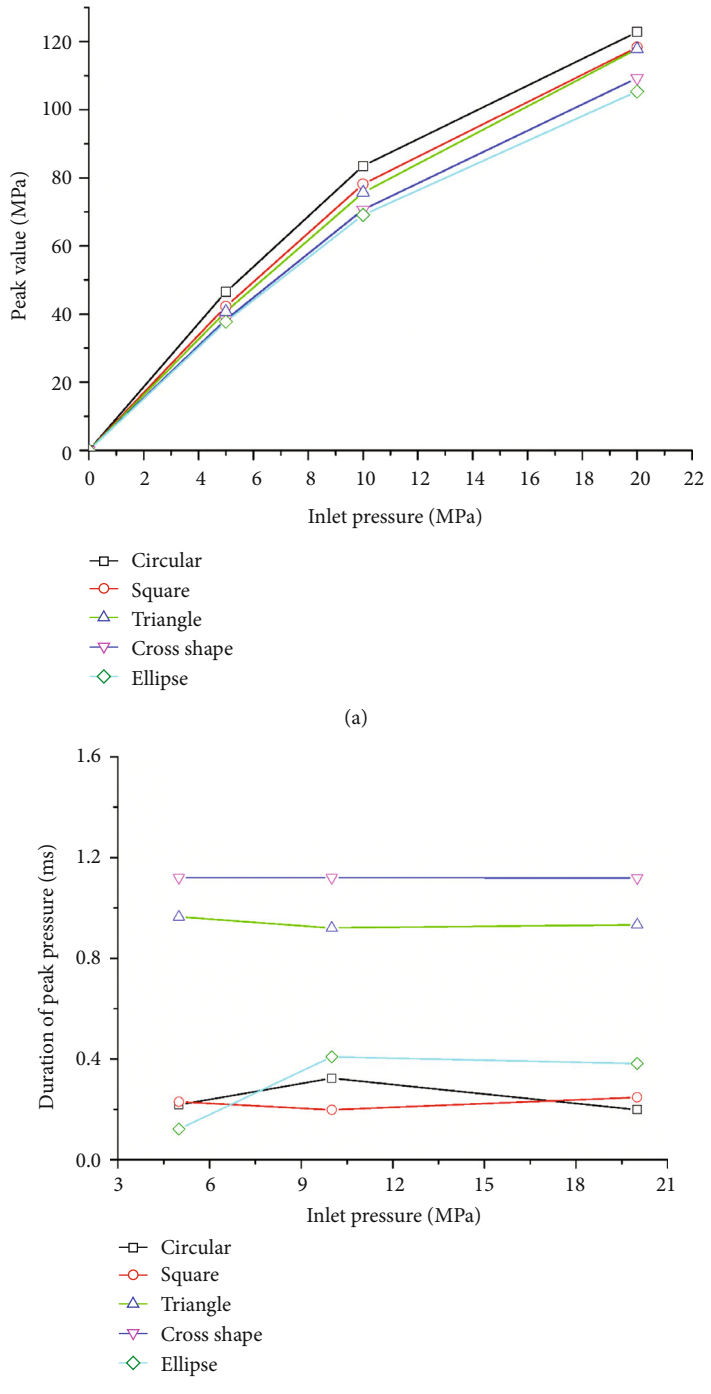

Figure 12: The relationship curve of peak pressure with jet inlet pressure.

regimes, the umbrella-like head shape of the circular water jet is not conducive to the generation of the lateral jet and may cause an extensive compression in the liquid. This compression may conversely act on the solid surface in the manner of an extremely high pressure. In contrast, the head shape of the elliptical jet is most conducive to the generation of the lateral jet and causes only a minor compression in liquid. Therefore, the center pressure induced by the compression behavior is sufficiently small. The flow regimes of the other three water jets indicate that their head shapes cause intermediate liquid compressions, which correspondingly induce the central pressures between the circular water jet and the elliptical water jet. The flow regimes also show an obvious central pressure distribution similar to that of the measured results. Accordingly, it is inferred that the discrepancy of the center pressure of different water jet shapes under the same inlet pressure may be a combined action of liquid velocities and jet head shapes.

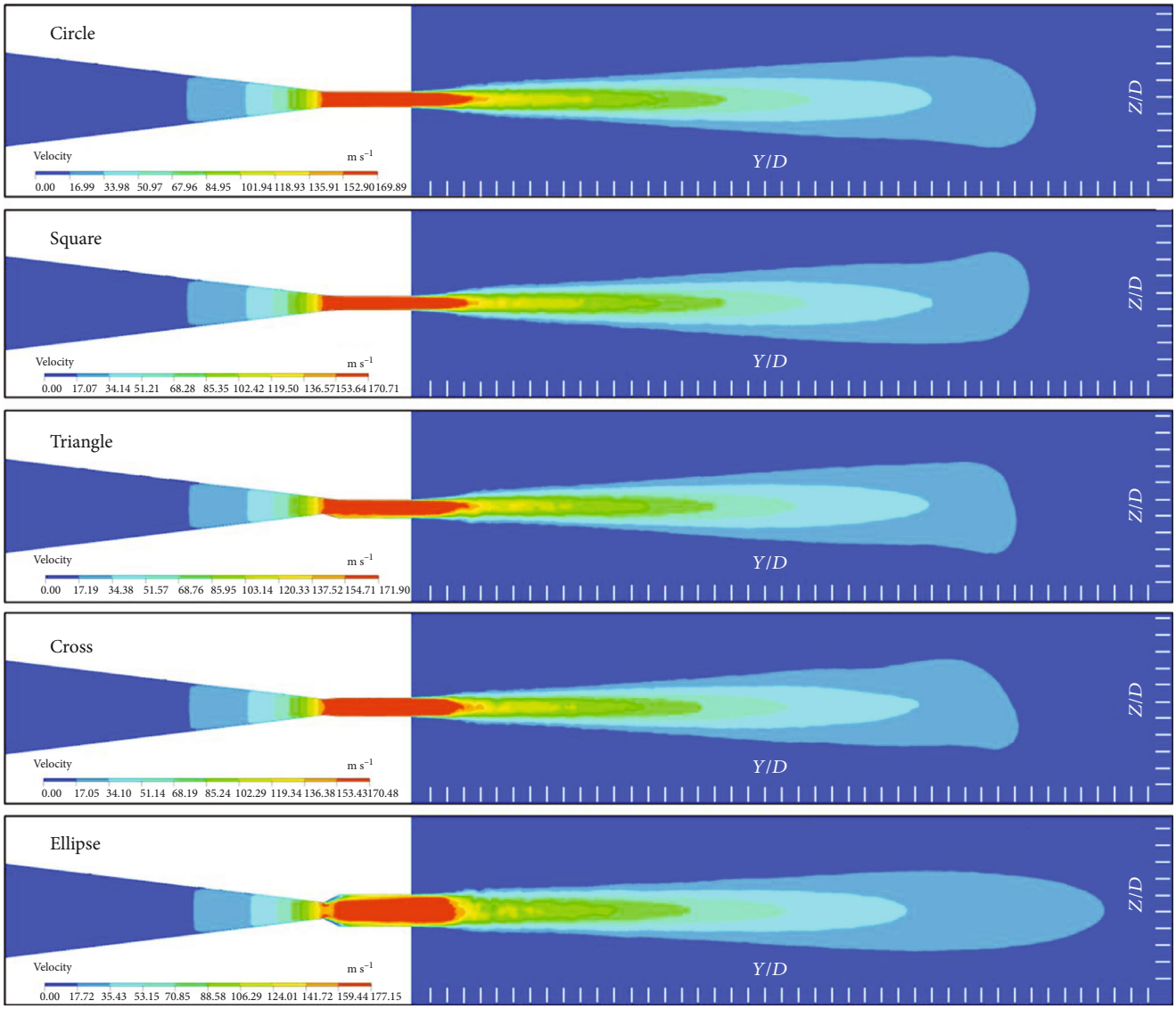

(a)

Figure 13: Continued.

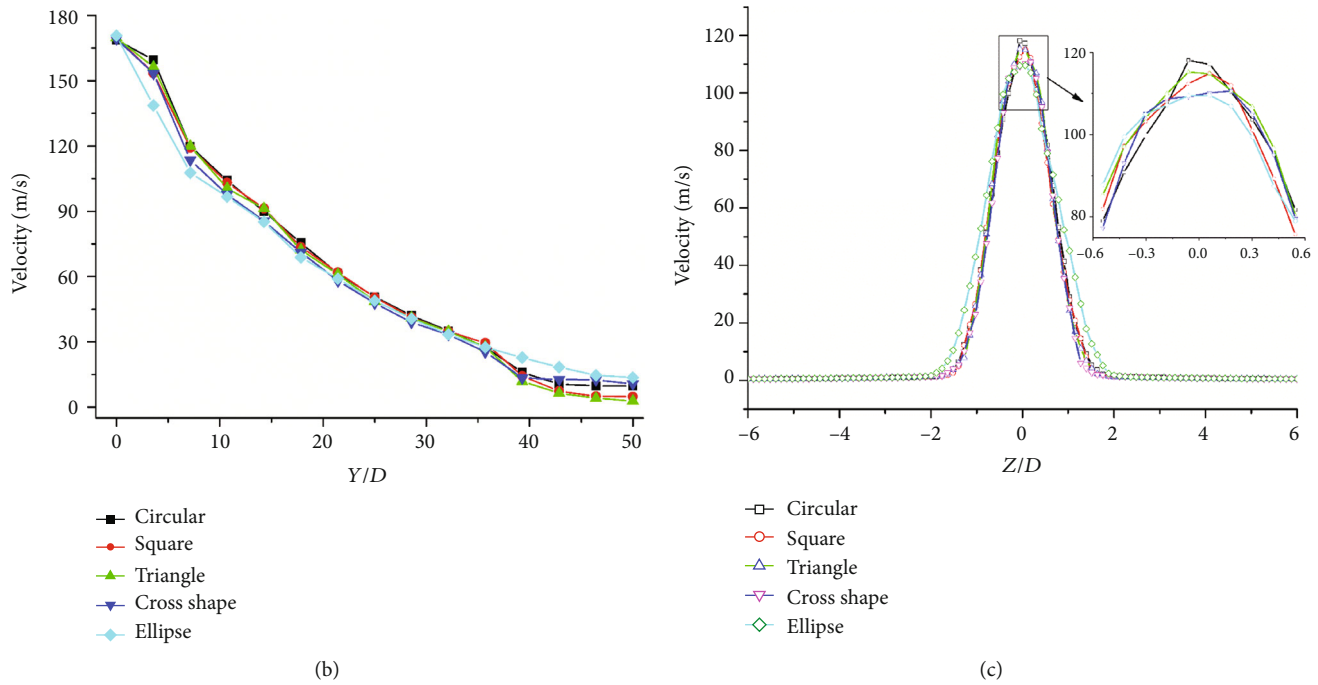

FIGURE 13: The velocity distributions of different water jets: (a) the velocity contours, (b) the axial velocity distribution, and (c) the radial velocity distribution.

5. Conclusions

A novel experimental platform with assistance from the CFD method was applied in this paper to study the impacting performance of high-pressure water jets from different nozzle orifices. The CFD results show that the cross-sections of different water jet shapes change from their original shapes to circular shapes with an increase in the axial distance. Hence, an optimal axial distance of approximately 15 millimeters was chosen in order to keep the same cross-section shapes as those of the designed nozzle shapes.

The PVDF testing results show that the central pressures of the different water jet shapes impacting onto the solid surface present a consistent pattern, namely, the initial transient and enormous peak pressure and then the longer and smaller stagnation pressure. The stagnation pressure in this paper is not sufficiently obvious and is thought to be the typical pressure profile of the pulsed water jet. The peak pressures of the five water jet shapes impacting onto solids are much different from one another. Under the same inlet pressure, the peak pressure of the circular water jet is the largest and those of the square, triangular, cross-shaped, and elliptical water jets decrease in turn. According to the flowing regimes captured by a high-speed camera, the umbrella-like head shape of the circular water jet is not conducive to the generation of a lateral jet and causes an extensive compression in the liquid. This compression may conversely act on the solid surface in the manner of an extremely high pressure. In contrast, the head shape of the elliptical jet is most conducive to the generation of the lateral jet and only causes tiny compressions in the liquid. The other three water jet shapes cause intermediate liquid compressions that correspondingly induce the central pressures between the circular water jet and the elliptical water jet. On the other hand, the velocity distribution maps show that the central velocity of the circular water jet is the highest, whereas that of the elliptical water jet is the lowest, and those of the square, triangular, and cross-shaped jets are in the middle. Accordingly, it is inferred that the discrepancy in the center pressure of the different water jet shapes under the same inlet pressure is a combined action of the liquid velocities and the jet head shapes. With an increase in the inlet pressure, the peak values of all of the water jet shapes increase nonlinearly while the durations are nearly kept constant.

Data Availability

All data included in this study are available upon request by contact with the corresponding author.

Conflicts of Interest

The authors declare no conflict of interest.

Acknowledgments

This work is jointly supported by the National Natural Science Foundation of China (No. 51804115) and the Natural Science Foundation of Hunan Province (No. 2016JJ4032).

References

[1] Y. Cho, S. Kim, H. Lim, S. Choi, and M. Kim, "Experimental study of electrostatic spray modes of high-flowrate water with horizontal nozzle," *Journal of Mechanical Science and Technology*, vol. 33, no. 9, pp. 4563–4572, 2019.

[2] G. Singh, T. Sundararajan, and K. A. Bhaskaran, "Mixing and entrainment characteristics of circular and noncircular confined jets," *Journal of Fluids Engineering*, vol. 125, no. 5, pp. 835–842, 2003.

[3] Y. Yu, C. LI, and H. Meng, "Flow and entrainment characteristics of jet from different shape nozzles," *The Chinese Journal of Process Engineering*, vol. 14, no. 4, pp. 549–555, 2014.

[4] M. Yang, S. Xiao, and C. Kang, "Influence of outlet profile on performance of central-body nozzle," *Fluid Machinery*, vol. 39, no. 5, pp. 13–19, 2011.

[5] E. Rouly, A. Warkentin, and R. Bauer, "Design and testing of low-divergence elliptical-jet nozzles," *Journal of Mechanical Science and Technology*, vol. 29, no. 5, pp. 1993–2003, 2015.

[6] E. Rouly, R. J. Bauer, and A. Warkentin, "An investigation into the effect of nozzle shape and jet pressure in profile creepfeed grinding," *Proceedings of the Institution of Mechanical Engineers, Part B: Journal of Engineering Manufacture*, vol. 231, no. 7, pp. 1116–1130, 2015.

[7] D. Singh, B. Premachandran, and S. Kohli, "Effect of nozzle shape on jet impingement heat transfer from a circular cylinder," *International Journal of Thermal Sciences*, vol. 96, pp. 45–69, 2015.

[8] K. Sodjavi, B. Montagné, P. Bragança, A. Meslem, F. Bode, and M. Kristiawan, "Impinging cross-shaped submerged jet on a flat plate: a comparison of plane and hemispherical orifice nozzles," *Meccanica*, vol. 50, no. 12, pp. 2927–2947, 2015.

[9] A. Ghasemi, V. Roussinova, R. Balachandar, and R. M. Barron, "Reynolds number effects in the near-field of a turbulent square jet," *Experimental Thermal and Fluid Science*, vol. 61, pp. 249–258, 2015.

[10] A. Hashiehbaf and G. P. Romano, "Particle image velocimetry investigation on mixing enhancement of non-circular sharp edge nozzles," *International Journal of Heat and Fluid Flow*, vol. 44, pp. 208–221, 2013.

[11] A. P. Vouros, T. Panidis, A. Pollard, and R. R. Schwab, "Near field vorticity distributions from a sharp-edged rectangular jet," *International Journal of Heat and Fluid Flow*, vol. 51, pp. 383–394, 2015.

[12] R. Vinze, S. Chandel, M. D. Limaye, and S. V. Prabhu, "Influence of jet temperature and nozzle shape on the heat transfer distribution between a smooth plate and impinging air jets," *International Journal of Thermal Sciences*, vol. 99, pp. 136–151, 2016.

[13] P. Sharma and T. Fang, "Spray and atomization of a common rail fuel injector with non-circular orifices," *Fuel*, vol. 153, pp. 416–430, 2015.

[14] W. R. Quinn, "Experimental study of the near field and transition region of a free jet issuing from a sharp-edged elliptic orifice plate," *European Journal of Mechanics - B/Fluids*, vol. 26, no. 4, pp. 583–614, 2007.

[15] F. Huang and B. Hu, "Macro/microbehavior of shale rock under the dynamic impingement of a high-pressure supercritical carbon dioxide jet," *RSC Advances*, vol. 8, no. 66, pp. 38065–38074, 2018.

[16] L.-L. Jiang, H.-K. Yin, X.-J. Li, and S.-W. Tang, "Fault Diagnosis of Rotating Machinery Based on Multisensor Information Fusion Using SVM and Time-Domain Features," *Shock and Vibration*, vol. 2014, Article ID 418178, 8 pages, 2014.

[17] D. Su, D. Zheng, and L. Zhao, "Experimental Study and Numerical Simulation of Dynamic Stress-Strain of Directional Blasting with Water Jet Assistance," *Shock and Vibration*, vol. 2019, Article ID 1659175, 15 pages, 2019.

[18] Y. Zhao, L. Zhang, W. Wang, Q. Liu, L. Tang, and G. Cheng, "Experimental study on shear behavior and a revised shear strength model for infilled rock joints," *International Journal of Geomechanics*, vol. 20, no. 9, article 04020141, 2020.

[19] A. Guha, R. M. Barron, and R. Balachandar, "An experimental and numerical study of water jet cleaning process," *Journal of Materials Processing Technology*, vol. 211, no. 4, pp. 610–618, 2011.

[20] S. Dehkhoda and M. Hood, "The internal failure of rock samples subjected to pulsed water jet impacts," *International Journal of Rock Mechanics and Mining Sciences*, vol. 66, pp. 91–96, 2014.

[21] https://dynasen.com/product-category/thin-film-sensors/.

[22] F. P. Bowden and J. E. Field, "The brittle fracture of solids by liquid impact, by solid impact, and by shock," *Proceedings of the Royal Society of London. Series A. Mathematical and Physical Sciences*, vol. 282, no. 1390, pp. 331–352, 1997.

[23] F. Huang, S. Li, Y. Zhao, and Y. Liu, "Study on lateral jetting range during an arc-curved jet impacting nonplanar solid surfaces," *Journal of Fluids Engineering*, vol. 140, no. 10, article 101201, 2018.

[24] Y. Liu, J. Wei, T. Ren, and Z. Lu, "Experimental study of flow field structure of interrupted pulsed water jet and breakage of hard rock," *International Journal of Rock Mechanics and Mining Sciences*, vol. 78, pp. 253–261, 2015.

[25] F. Huang, S. Li, Y. Zhao, and Y. Liu, "A numerical study on the transient impulsive pressure of a water jet impacting nonplanar solid surfaces," *Journal of Mechanical Science and Technology*, vol. 32, no. 9, pp. 4209–4221, 2018.

[26] D. Su, Y. Kang, D. Li, X. Wang, and F. Yan, "Analysis and numerical simulation on the reduction effect of stress waves caused by water jet slotting near blasting source," *Shock and Vibration*, vol. 2016, Article ID 5640947, 18 pages, 2016.

[27] X. Xu, J. Ouyang, T. Jiang, and Q. Li, "Numerical analysis of the impact of two droplets with a liquid film using an incompressible SPH method," *Journal of Engineering Mathematics*, vol. 85, no. 1, pp. 35–53, 2014.

[28] J. Q. Feng, "A computational study of high-speed microdroplet impact onto a smooth solid surface," *Journal of Applied Fluid Mechanics*, vol. 10, no. 1, pp. 243–256, 2017.

[29] C.-Y. Hsu, C.-C. Liang, T.-L. Teng, and A.-T. Nguyen, "A numerical study on high-speed water jet impact," *Ocean Engineering*, vol. 72, pp. 98–106, 2013.

[30] D. Li, Y. Kang, X. Ding, X. Wang, and Z. Fang, "An experimental investigation on the pressure characteristics of high speed self-resonating pulsed waterjets influenced by feeding pipe diameter," *Journal of Mechanical Science and Technology*, vol. 30, no. 11, pp. 4997–5007, 2016.

[31] M. B. Lesser and J. E. Field, "The impact of compressible liquids," *Annual Review of Fluid Mechanics*, vol. 15, no. 1, pp. 97–122, 1983.

[32] F. J. Heymann, "On the shock wave velocity and impact pressure in high-speed liquid-solid impact," *Journal of Basic Engineering*, vol. 90, no. 3, pp. 400–402, 1968.